J. Fluid Mech. (1995), *vol.* 285, *pp.* 203–214

On the viscous decay rates of inertial waves in a rotating circular cylinder

By R. R. KERSWELL AND C. F. BARENGHI
Department of Mathematics and Statistics, University of Newcastle upon Tyne, NE1 7RU, UK

(Received 3 June 1994 and in revised form 1 August 1994)

In the literature, there are two different asymptotic results for the viscous decay rates of inertial modes in a rotating circular cylinder. In the absence of a viscous corner solution, either result can only be an estimate of the true decay rate. In this note, we numerically calculate the viscous decay rates for some experimentally excited inertial modes (Malkus 1989; Malkus & Waleffe 1991) in order to (i) assist in the interpretation of these experiments and (ii) to assess the usefulness of the two asymptotic estimates available. Our results indicate that the asymptotic estimate due to Kudlick (1966) is more accurate and that the asymptotic regime in which this estimate is useful (accurate to within 10%) can be smaller than is commonly thought.

1. Introduction

It is well known that inertial oscillations with a frequency less than twice the basic rotation rate can exist within a uniformly rotating fluid. The dispersion relation for the modal eigenfrequencies in a cylinder was first derived by Kelvin (1880) and subsequently confirmed experimentally by Bjerknes *et al.* (1933), Fultz (1959), McEwan (1970), Stergiopoulos & Aldridge (1982) and more recently Manasseh (1992, 1994). A large body of literature now exists cataloguing how such modes may be resonantly excited under various conditions within a rotating cylinder (see Manasseh 1992, 1994 for the main references). Practically, one of the more familiar manifestations of inertial wave resonance is the instability of fluid-filled gyroscopes or spinning projectiles (Stewartson 1959) which occurs when the nutational frequency is tuned to an inertial wave frequency (e.g. Karpov 1965).

A number of authors have studied the viscous modification of these inertial waves within a cylinder in terms of the Ekman boundary layers which form and the possibility of viscous shear layers along the characteristic directions (Wood 1965, 1966; Kudlick 1966; Wedemeyer 1966; Baines 1967; Johnson 1967; Gans 1970; McEwan 1970). Out of this body of work, two different asymptotic estimates for the modal viscous decay rates in a cylinder have emerged. These estimates differ in the way they treat the corner regions of the cylinder where the Ekman layer scalings no longer hold. One estimate due to Kudlick (1966) assumes that the corners are sufficiently rounded for an Ekman layer to negotiate them without need for rescaling. The other, due to Wedemeyer (1966), completely ignores the need for joining corner regions by calculating the decay rate contributions for the horizontal and vertical Ekman layers separately. Both neglect the possible effect of viscous shear layers emanating out of the corner regions as first suggested analytically by Wood (1965, 1966), more recently by Kerswell (1994*b*), and seen experimentally by McEwan (1970) and Manasseh (1992), albeit only in certain circumstances.

Unfortunately, there has been no definitive experimental work to identify which is the more valuable estimate, due in part to the difficulty of measuring decay rates accurately. A series of experiments, carried out at the US Ballistic Research Laboratory and summarized by Whiting & Gerber (1980), compared Wedemeyer's asymptotic result with experimental measurements of the motion of liquid-filled gyroscopes, reporting agreement to within 10% for Ekman numbers below 10^{-4} and only 25% above 10^{-4}. In a related but separate vein, Stergiopoulos & Aldridge (1987) and Aldridge & Stergiopoulos (1991) have developed techniques for measuring the complex eigenfrequencies of inertial modes *while* the fluid is spun up from rest, motivated by the fluid-filled projectile problem. Unfortunately, their results are not directly relevant here.

It is therefore the purpose of this note to numerically estimate the viscous decay rates of a few select inertial modes in order to assess the accuracy of the two available asymptotic estimates. Our choice of particular inertial modes and cylindrical geometries to study is motivated by a series of ongoing experiments in which a flow set up within an elliptically-distorted, rotating cylinder is observed to bifurcate through the excitation of inertial waves (Malkus 1989; Malkus & Waleffe 1991). Two inertial modes are found to be elliptically excited if (i) their azimuthal wavenumbers—differ by two, (ii) their frequencies (non-dimensionalized by the rotation rate) differ by two, and (iii) their axial wavenumbers are similar.

For the lowest subharmonic resonance where an $m = 1$ mode couples with its complex conjugate (model $l = n = 1$ in table 1), the asymptotic estimates differ by fully 20%. It is this particular discrepancy and efforts to study the weakly nonlinear evolution of this elliptical resonance which were instrumental in initiating the present numerical study. Specifically, if the horizontal and vertical Ekman layers can be treated in isolation, that is, the corners are unimportant (Wedemeyer's estimate), then the boundary-layer-driven $O(E^{1/2})$ internal viscous flow can be found as a closed analytic form. Conversely, if the corner regions *are* important (as in Kudlick's estimate), this leading-order viscous flow can only be obtained as part of a full numerical solution found here.

Table 2 contains the decay rate results for a challenger ($l = n = 3$) to the lowest-order ($l = m = n = 1$) resonance. Table 3 contains the decay rates for the second subharmonic resonance ($l = n = 2$), and tables 4 and 5 the relevant decay rates for the lowest-order ($l = n = 1$) $m = (0, +2)$ elliptical resonance. As the point of bifurcation in these experiments is determined by the balance between the joint elliptical growth rate of the wave pair and the geometric mean of their individual viscous decay rates (Kerswell 1994*a*), the results presented here are then directly testable.

The paper is organized as follows. Section 2 introduces the inertial wave problem for a rotating cylinder and describes the two asymptotic estimates for their viscous decay rates. Section 3 presents the numerical formulation of the problem and §4 discusses the numerical results.

2. Asymptotic decay rate estimates

The linearized equations for describing small motions of a viscous, incompressible fluid away from uniform rotation are

$$\frac{\partial \boldsymbol{u}}{\partial t} + 2\hat{\boldsymbol{k}} \times \boldsymbol{u} + \nabla p = E\nabla^2 \boldsymbol{u}, \tag{2.1}$$

$$\nabla \cdot \boldsymbol{u} = 0, \tag{2.2}$$

in the rotating frame. The basic rotation rate Ω and cylindrical radius R have been used to non-dimensionalize the system, with the Ekman number $E = \nu/\Omega R^2$ appearing as the non-dimensionalization of the kinematic viscosity ν. The boundary conditions are those of non-slip on the cylindrical surface which is at rest in the rotating frame,

$$\boldsymbol{u} = \boldsymbol{0} \quad \text{on} \quad z = 0, d \quad \text{and} \quad r = 1. \tag{2.3}$$

The inviscid limit, in which E is set to zero and the non-slip boundary conditions are relaxed to a no-normal-velocity condition, gives rise to the inertial wave problem, where wave solutions

$$[\boldsymbol{u}, p] = [u(r,z), v(r,z), w(r,z), \Phi(r,z)]\, \mathrm{e}^{\mathrm{i}(m\phi+\lambda t)}$$

may be sought. The reduction of the problem to one for only the pressure realizes the Poincaré equation

$$\frac{1}{r}\frac{\partial}{\partial r} r \frac{\partial \Phi}{\partial r} - \frac{m^2}{r^2}\Phi + \left(1 - \frac{4}{\lambda^2}\right)\frac{\partial^2 \Phi}{\partial z^2} = 0 \tag{2.4}$$

to be solved subject to the boundary conditions

$$\frac{\partial \Phi}{\partial r} + \frac{2m}{\lambda r}\Phi = 0 \quad \text{on} \quad r = 1,$$

$$\frac{\partial \Phi}{\partial z} = 0 \quad \text{on} \quad z = 0, d.$$

Separable solutions exist of the form

$$\boldsymbol{u} = \frac{\mathrm{e}^{\mathrm{i}(m\phi+\lambda t)}}{2(4-\lambda^2)} \begin{bmatrix} \mathrm{i}\{(\lambda+2)J_{m-1}(kr) - (\lambda-2)J_{m+1}(kr)\}\cos(l\pi z/d) \\ -\{(\lambda+2)J_{m-1}(kr) + (\lambda-2)J_{m+1}(kr)\}\cos(l\pi z/d) \\ 2\mathrm{i}\lambda k d(\pi l)^{-1} J_m(kr)\sin(l\pi z/d) \end{bmatrix}, \tag{2.5}$$

$$p = -\frac{1}{k} J_m(kr)\cos(l\pi z/d)\, \mathrm{e}^{\mathrm{i}(m\phi+\lambda t)}, \tag{2.6}$$

where

$$\lambda = \frac{\pm 2}{[1 + k^2 d^2/(\pi l)^2]^{1/2}},$$

and k is a solution, indexed by n such that $0 < k_{n=1} < k_{n=2} \ldots$, of

$$r\frac{\mathrm{d}}{\mathrm{d}r} J_m(kr) + \frac{2m}{\lambda} J_m(kr) = 0|_{r=1}.$$

Three numbers, l, $n \in \mathcal{N}$, and $m \in \mathcal{M}$, are sufficient to specify the inertial mode and in particular the frequency $\lambda = \lambda_{lmn}$. These indices correspond roughly with the number of nodes axially, radially and azimuthally, respectively, in the pressure eigenfunction.

The now well-established corrective procedure to accommodate small but finite values of the Ekman number is to fit an $E^{1/2}$ boundary layer to the inertial mode (Greenspan 1968). Typically, the following expansions are used:

$$\begin{aligned} \boldsymbol{u} &= \boldsymbol{u}_0 + \tilde{\boldsymbol{u}}_0 + E^{1/2}(\boldsymbol{u}_1 + \tilde{\boldsymbol{u}}_1) + \ldots, \\ p &= p_0 + \tilde{p}_0 + E^{1/2}(p_1 + \tilde{p}_1) + \ldots, \\ \partial/\partial t &= \mathrm{i}\lambda + E^{1/2} s + \ldots, \end{aligned}$$

where $[\boldsymbol{u}_0, p_0]$ is the inertial wave, the tilde indicates a boundary layer variable and

$-\mathrm{Re}(E^{1/2}s)$ is the viscous decay rate. Application of the solvability condition to the $O(E^{1/2})$ interior equations (see Greenspan 1968, §2.9), leads to an expression for the viscous (complex) frequency shift

$$s = \frac{-\iint \mathrm{d}S p_0^* \boldsymbol{u}_1 \cdot \hat{\boldsymbol{n}}}{\iiint |\boldsymbol{u}_0|^2 \,\mathrm{d}V} = \frac{-\iint \mathrm{d}S p_0^* \int_0^\infty \hat{\boldsymbol{n}} \cdot \boldsymbol{\nabla} \times (\hat{\boldsymbol{n}} \times \tilde{\boldsymbol{u}}_0)\,\mathrm{d}\xi}{\iiint |\boldsymbol{u}_0|^2 \,\mathrm{d}V}, \tag{2.7}$$

where ξ is the rescaled variable normal to the surface, i.e. $\hat{\boldsymbol{n}} \cdot \boldsymbol{\nabla} = -E^{-1/2}\partial/\partial\xi$. The leading boundary equations are readily solved in terms of the inviscid inertial wave structure,

$$\hat{\boldsymbol{n}} \times \tilde{\boldsymbol{u}}_0 \pm \mathrm{i}\tilde{\boldsymbol{u}}_0 = -(\hat{\boldsymbol{n}} \times \boldsymbol{u}_0 \pm \mathrm{i}\boldsymbol{u}_0) \exp\{-\xi[\mathrm{i}(\lambda \pm 2\hat{\boldsymbol{n}} \cdot \hat{\boldsymbol{k}})]^{1/2}\}, \tag{2.8}$$

where this is just the time-dependent version of Greenspan's (1968) equation 2.6.12. The decay rate expression (2.7) can be evaluated directly by assuming that an Ekman layer exists everywhere over the cylindrical surface including the corners. This assumption necessarily means that the horizontal Ekman layers fit discontinuously onto the vertical Ekman layers in the corner regions. Following this prescription, however, leads to Wedemeyer's expression

$$s_1 = \frac{-(4-\lambda^2)[m^2+(\pi l/d)^2]}{4\sqrt{2}\,d[m^2+(\pi l/d)^2-m\lambda/2]} \left\{ \frac{(2-\lambda)(1+\mathrm{i})}{(2+\lambda)^{1/2}} + \frac{(2+\lambda)(1-\mathrm{i})}{(2-\lambda)^{1/2}} + \frac{\lambda d(1+\mathrm{i})}{\lambda^{1/2}} \right\}. \tag{2.9}$$

The formula has been derived for $\lambda > 0$; extension to $\lambda < 0$ follows from $s(m, \lambda) = s^*(-m, -\lambda)$.

Kudlick's estimate derives from rewriting (2.7) as

$$s = \frac{-\iint \mathrm{d}S p_0^* \boldsymbol{u}_1 \cdot \hat{\boldsymbol{n}}}{\iiint |\boldsymbol{u}_0|^2 \,\mathrm{d}V} = \frac{\iint \mathrm{d}S \boldsymbol{\nabla} p_0^* \cdot \int_0^\infty \tilde{\boldsymbol{u}}_0 \,\mathrm{d}\xi - \iint \mathrm{d}\boldsymbol{S} \cdot \boldsymbol{\nabla} \times \int_0^\infty \mathrm{d}\xi [p_0^* (\hat{\boldsymbol{n}} \times \tilde{\boldsymbol{u}}_0)]}{\iiint |\boldsymbol{u}_0|^2 \,\mathrm{d}V} \tag{2.10}$$

and then neglecting the last term of the numerator by appeal to the Divergence theorem to get the expression

$$s_2 = \frac{-1}{4\sqrt{2}\iiint |\boldsymbol{u}_0|^2 \,\mathrm{d}V} \iint \mathrm{d}S \left\{ |\sigma_+|^{1/2} \left[1 + \frac{\mathrm{i}\sigma_+}{|\sigma_+|} \right] |\boldsymbol{u}_0 - \mathrm{i}\hat{\boldsymbol{n}} \times \boldsymbol{u}_0|^2 \right.$$

$$\left. + |\sigma_-|^{1/2} \left[1 + \frac{\mathrm{i}\sigma_-}{|\sigma_-|} \right] |\boldsymbol{u}_0 + \mathrm{i}\hat{\boldsymbol{n}} \times \boldsymbol{u}_0|^2 \right\}, \tag{2.11}$$

where $\sigma_\pm = (\lambda \pm 2\hat{\boldsymbol{n}} \cdot \hat{\boldsymbol{k}})$. This is the cylindrical analogue of Greenspan's (1968) general result, expression 2.9.13. Evaluation leads to Kudlick's estimate

$$s_2 = \frac{-(4-\lambda^2)}{4\sqrt{2}\,d[m^2+(\pi l/d)^2-m\lambda/2]} \left\{ (1+\mathrm{i}) \frac{2-\lambda}{(2+\lambda)^{1/2}} \left[m^2 + \left(\frac{\pi l}{d}\right)^2 - \frac{2m\lambda}{2-\lambda} \right] \right.$$

$$+ (1-\mathrm{i}) \frac{2+\lambda}{(2-\lambda)^{1/2}} \left[m^2 + \left(\frac{\pi l}{d}\right)^2 - \frac{2m\lambda}{2+\lambda} \right] + (1+\mathrm{i}) \left[m^2 + \left(\frac{\pi l}{d}\right)^2 \right] \left. \mathrm{d}\lambda^{1/2} \right\}. \tag{2.12}$$

This procedure implicitly assumes that the integrand,

$$\hat{\boldsymbol{n}} \cdot \boldsymbol{\nabla} \times \int_0^\infty \mathrm{d}\xi [p_0^* (\hat{\boldsymbol{n}} \times \tilde{\boldsymbol{u}}_0)],$$

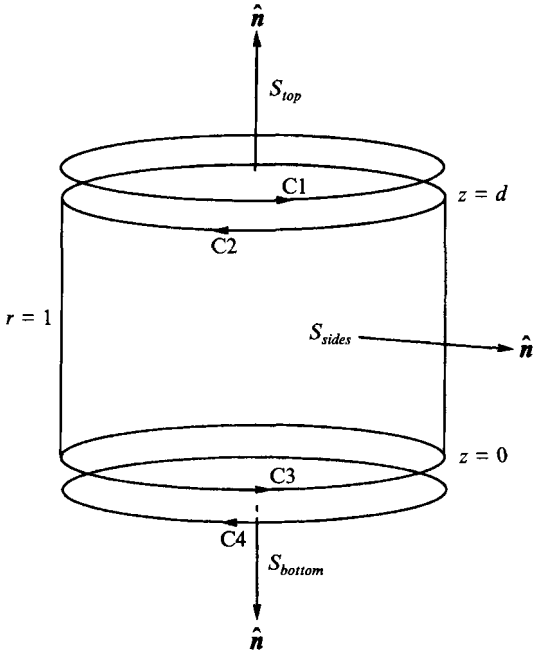

FIGURE 1. The line integrals $\oint \mathrm{d}\boldsymbol{r} \cdot \int_0^\infty \mathrm{d}\xi p_0^*(\hat{\boldsymbol{n}} \times \tilde{\boldsymbol{u}}_0)$ along C1 and C2 (and likewise C3 and C4) did not cancel owing to the different normals of their attached surfaces.

is a smooth continuous function over the closed surface. In view of the dependence of the boundary layer solution upon the surface normal vector (2.8), this condition is actually a restriction upon the surface. For Kudlick's assumption to hold, the geometry must have a *smooth* surface upon which the normal varies *continuously* and clearly a cylinder does not possess this property (see figure 1). In effect, Kudlick treats the corners as significantly rounded, i.e. that the radius of curvature is large compared to $RE^{-1/2}$. Then there are no corners but rather a continuously varying Ekman layer over the entire cylindrical surface.

The reader should note that

$$-\mathrm{Re}(s_1) + \mathrm{Re}(s_2) = \frac{(4-\lambda^2)m\lambda}{2\sqrt{2}[m^2 + (\pi l/d)^2 - m\lambda/2]} \left\{ \frac{1}{(2+\lambda)^{1/2}} + \frac{1}{(2-\lambda)^{1/2}} \right\} \tag{2.13}$$

so that Wedemeyer's estimate for the decay rate is never less than Kudlick's for $m\lambda \geqslant 0$ and the two asymptotic estimates are equal at $m = 0$.

3. Numerical formulation

The equations to be solved are (2.1) and (2.2) subject to (2.3). Axisymmetric and non-axisymmetric solutions are sought separately. The streamfunction decomposition

$$\boldsymbol{u} = \nabla \times \left[\frac{\psi(r,z)}{r} \hat{\boldsymbol{\phi}} \right] + v(r,z)\hat{\boldsymbol{\phi}} = \left[-\frac{\psi_z}{r}, v, \frac{\psi_r}{r} \right] \tag{3.1}$$

is used in the axisymmetric case, leading to the equations

$$\frac{\partial}{\partial t}\left[\frac{\psi_r}{r^2} - \frac{\psi_{zz}}{r} - \frac{\psi_{rr}}{r} \right] = 2v_z + E\left\{ -\frac{\psi_{rrrr}}{r} - 2\frac{\psi_{rrzz}}{r} - \frac{\psi_{zzzz}}{r} + 2\frac{\psi_{rrr}}{r^2} + 2\frac{\psi_{rzz}}{r^2} - 3\frac{\psi_{rr}}{r^3} + 3\frac{\psi_r}{r^4} \right\}, \tag{3.2}$$

$$\frac{\partial v}{\partial t} = 2\frac{\psi_z}{r} + E\left\{v_{rr} + v_{zz} + \frac{v_r}{r} - \frac{v}{r^2}\right\}, \tag{3.3}$$

to be solved subject to the boundary conditions

$$\psi = \psi_r = v = 0 \quad \text{at} \quad r = 1, \tag{3.4}$$

$$\psi = \psi_z = v = 0 \quad \text{at} \quad z = 0, d. \tag{3.5}$$

In the asymmetric case, we work with the radial and axial velocities u and w, using the incompressibility condition and the azimuthal component of the momentum equation to eliminate the azimuthal velocity and pressure. This leaves the equations

$$\frac{\partial}{\partial t}[r^2 u_{rr} + 3ru_r + (1-m^2)u + r^2 w_{rz} + 2rw_z] = -2imrw_z$$

$$+ E\left\{r^2 u_{rrrr} + r^2 u_{rrzz} + 6ru_{rrr} + 3ru_{rzz} + (5-2m^2)u_{rr} + (1-m^2)u_{zz} - (2m^2+1)\frac{u_r}{r}\right.$$

$$\left. + (m^2-1)^2\frac{u}{r^2} + r^2 w_{rrrz} + r^2 w_{rzzz} + 2rw_{zzz} + 5rw_{rrz} + (3-m^2)w_{rz} - 2\frac{m^2 w_z}{r}\right\}, \tag{3.6}$$

$$\frac{\partial}{\partial t}[r^2 u_{rz} + ru_z + r^2 w_{zz} - m^2 w] = 2imru_z$$

$$+ E\left\{r^2 u_{rrrz} + r^2 u_{rzzz} + 4ru_{rrz} + ru_{zzz} + (1-m^2)\left(u_{rz} - \frac{u_z}{r}\right) + r^2 w_{rrzz}\right.$$

$$\left. + r^2 w_{zzzz} + 3rw_{rzz} - m^2\left(w_{rr} + 2w_{zz} + \frac{w_r}{r} - \frac{m^2 w}{r^2}\right)\right\}, \tag{3.7}$$

where the exponential factor $e^{im\phi}$ has been suppressed, to be solved subject to the boundary conditions

$$u = u_r = w = 0 \quad \text{at} \quad r = 1, \tag{3.8}$$

$$u = w = w_z = 0 \quad \text{at} \quad z = 0, d. \tag{3.9}$$

We use two types of spectral functions built up as appropriate linear combinations of Chebyshev polynomials $T_n(x) = \cos(n\cos^{-1}x)$ so that they satisfy the required boundary conditions:

$$\Theta_n(x) = T_n(x) - \frac{2(n-2)}{n-3}T_{n-2}(x) + \frac{n-1}{n-3}T_{n-4}(x) \tag{3.10}$$

which satisfies $\Theta_n(1) = \dfrac{d\Theta_n}{dx}(1) = 0 \quad \text{for} \quad n \geqslant 4,$

and

$$\Psi_n(x) = T_n(x) - T_{n-2}(x) \tag{3.11}$$

which satisfies $\Psi_n(1) = 0 \quad \text{for} \quad n \geqslant 2.$

Chebyshev polynomials are chosen as the basis functions owing to their well-known ability to represent a rapidly varying function at the boundary economically. We can anticipate needing only $O(E^{-1/4})$ spectral modes in each direction to resolve the $O(E^{1/2})$ layers on the horizontal and vertical surfaces, requiring $O(E^{-1})$ storage in total. It is worth remarking that both sets of equations ((3.2)–(3.7)) are independent of z, suggesting the use of Fourier expansion functions, and the possibility of a banded discretization matrix. Hollerbach (1994) has used just such a technique with

considerable success working in a spherical shell. However, owing to their uniform wavelength throughout the domain, we would need $O(E^{-1/2})$ of them to resolve the top and bottom boundary layers and consequently there would be no obvious gain in storage space. Moreover, imposing the vertical boundary conditions while still preserving the banded matrix structure adds further complications to this approach.

We exploit the symmetries of the inertial waves by actually solving the equations only in the upper 'quadrant' $\{0 \leqslant r \leqslant 1; d/2 \leqslant z \leqslant d\}$ of an extended cylinder viewed as the domain $\{-1 \leqslant r \leqslant 1; 0 \leqslant z \leqslant d\}$. If m is even (odd), then w, ψ are even (odd) and u, v are odd (even) functions of r. Likewise about the cylindrical equator $z = d/2$, if l is even (odd), then u, v are even (odd) and w, ψ are odd (even) functions of

$$z^* = \frac{2z}{d} - 1. \tag{3.12}$$

Hence, for example, in the case when $m = l = 1$ the spectral expansions used are as follows:

$$u = \sum_{i=1}^{N} \sum_{j=1}^{M} a_{ij}\, \Theta_{2i+2}(r)\, \Psi_{2j+1}(z^*), \quad w = \sum_{i=1}^{N} \sum_{j=1}^{M} b_{ij}\, \Psi_{2i+1}(r)\, \Theta_{2j+2}(z^*), \tag{3.13}$$

and for $m = 0, l = 1$,

$$\psi = \sum_{i=1}^{N} \sum_{j=1}^{M} a_{ij}\, \Theta_{2i+2}(r)\, \Theta_{2j+2}(z^*), \quad v = \sum_{i=1}^{N} \sum_{j=1}^{M} b_{ij}\, \Psi_{2i+1}(r)\, \Psi_{2j+1}(z^*). \tag{3.14}$$

The equations are then collocated in the radial direction using the N positive zeros of $T_{2N}(r)$, and in the axial direction using the M positive zeros of $T_{2M}(z^*)$. This recipe ensures that the collocation points are concentrated where the solution varies most rapidly, that is, at the top and side boundaries and the corner region.

We are interested in evaluating the viscous decay rates of the low-wavenumber modes. Unfortunately, there is no guarantee that these decay rates will be the smallest because a higher-wavenumber mode, concentrated in the bulk interior, can have a weaker boundary layer and hence decay rate (e.g. see tables 1 and 2). This prevents us from simply time-stepping equations (3.2)–(3.7) starting with an arbitrary initial state. Instead, we are forced to solve an eigenvalue problem. The equations are integrated forward in time by one step Δt using the second-order implicit Crank–Nicholson method which leads to the mapping

$$\boldsymbol{A}\boldsymbol{x}^{n+1} = \boldsymbol{B}\boldsymbol{x}^{n} \tag{3.15}$$

where $\boldsymbol{x}^n$ is the vector of spectral coefficients at time t^n and the matrices $\boldsymbol{A}$ and $\boldsymbol{B}$ are $2NM \times 2NM$, dense and complex (real) in the asymmetric (axisymmetric) case. Once the eigenvalues μ of the matrix $\boldsymbol{A}^{-1}\boldsymbol{B}$ are obtained via the appropriate NAG routine, the complex frequencies σ trivially follow by inverting the relation

$$\mu = \mathrm{e}^{\sigma \Delta t}.$$

This method requires that the convergence in Δt be checked as well as the effect of the truncations N and M. Such convergence is readily achieved, with typically $\Delta t = 10^{-4}$ proving sufficient. The advantage of this implicit-time-stepping method is that it prevents the appearance of spurious eigenvalues.

4. Results

Numerically, the problem of reaching down to the experimental Ekman numbers of $E \leqslant 10^{-4}$, at which the asymptotic decay rate estimates should make sense, is an ambitious one. Even with a given azimuthal wavenumber, the problem is two-

E	$n=1$	$n=2$	$n=3$
5×10^{-3}	$1.004\mathrm{i}-2.319E^{1/2}$	$0.508\mathrm{i}-4.456E^{1/2}$	$0.327\mathrm{i}-8.045E^{1/2}$
2×10^{-3}	$1.003\mathrm{i}-1.985E^{1/2}$	$0.509\mathrm{i}-3.287E^{1/2}$	$0.337\mathrm{i}-5.530E^{1/2}$
1×10^{-3}	$1.002\mathrm{i}-1.823E^{1/2}$	$0.509\mathrm{i}-2.723E^{1/2}$	$0.338\mathrm{i}-4.260E^{1/2}$
5×10^{-4}	$1.001\mathrm{i}-1.712E^{1/2}$	$0.510\mathrm{i}-2.334E^{1/2}$	$0.338\mathrm{i}-3.385E^{1/2}$
2×10^{-4}	$1.001\mathrm{i}-1.615E^{1/2}$	$0.511\mathrm{i}-1.996E^{1/2}$	$0.339\mathrm{i}-2.630E^{1/2}$
1×10^{-4}	$1.001\mathrm{i}-1.566E^{1/2}$	$0.511\mathrm{i}-1.829E^{1/2}$	$0.339\mathrm{i}-2.256E^{1/2}$
5×10^{-5}	$1.000\mathrm{i}-1.532E^{1/2}$	$0.511\mathrm{i}-1.712E^{1/2}$	$0.340\mathrm{i}-1.994E^{1/2}$
2×10^{-5}	$1.000\mathrm{i}-1.500E^{1/2}$	$0.512\mathrm{i}-1.610E^{1/2}$	$0.340\mathrm{i}-1.764E^{1/2}$
1×10^{-5}	$1.000\mathrm{i}-1.483E^{1/2}$	$0.512\mathrm{i}-1.563E^{1/2}$	$0.340\mathrm{i}-1.650E^{1/2}$
Wedemeyer's estimate	$-1.732E^{1/2}$	$-1.585E^{1/2}$	$-1.474E^{1/2}$
Kudlick's estimate	$-1.451E^{1/2}$	$-1.432E^{1/2}$	$-1.373E^{1/2}$

TABLE 1. Frequencies $\sigma = \mathrm{i}\lambda + E^{1/2}s$ for $d = 1.9898$ and $m = l = 1$

E	$n=1$	$n=2$	$n=3$
5×10^{-3}	$1.789\mathrm{i}-3.209E^{1/2}$	$1.302\mathrm{i}-5.548E^{1/2}$	$0.950\mathrm{i}-9.083E^{1/2}$
2×10^{-3}	$1.789\mathrm{i}-2.248E^{1/2}$	$1.300\mathrm{i}-3.948E^{1/2}$	$0.955\mathrm{i}-6.190E^{1/2}$
1×10^{-3}	$1.787\mathrm{i}-1.803E^{1/2}$	$1.297\mathrm{i}-3.169E^{1/2}$	$0.953\mathrm{i}-4.776E^{1/2}$
5×10^{-4}	$1.784\mathrm{i}-1.501E^{1/2}$	$1.295\mathrm{i}-2.629E^{1/2}$	$0.952\mathrm{i}-3.795E^{1/2}$
2×10^{-4}	$1.781\mathrm{i}-1.241E^{1/2}$	$1.293\mathrm{i}-2.156E^{1/2}$	$0.951\mathrm{i}-2.938E^{1/2}$
1×10^{-4}	$1.779\mathrm{i}-1.112E^{1/2}$	$1.292\mathrm{i}-1.921E^{1/2}$	$0.951\mathrm{i}-2.510E^{1/2}$
5×10^{-5}	$1.778\mathrm{i}-1.022E^{1/2}$	$1.291\mathrm{i}-1.755E^{1/2}$	$0.950\mathrm{i}-2.209E^{1/2}$
2×10^{-5}	$1.777\mathrm{i}-0.943E^{1/2}$	$1.290\mathrm{i}-1.610E^{1/2}$	$0.950\mathrm{i}-1.943E^{1/2}$
1×10^{-5}	$1.777\mathrm{i}-0.904E^{1/2}$	$1.290\mathrm{i}-1.537E^{1/2}$	$0.950\mathrm{i}-1.812E^{1/2}$
Wedemeyer's estimate	$-0.840E^{1/2}$	$-1.399E^{1/2}$	$-1.525E^{1/2}$
Kudlick's estimate	$-0.809E^{1/2}$	$-1.359E^{1/2}$	$-1.490E^{1/2}$

TABLE 2. Frequencies $\sigma = \mathrm{i}\lambda + E^{1/2}s$ for $d = 1.9898$, $m = 1$ and $l = 3$

E	$n=1$	$n=2$	$n=3$
5×10^{-3}	$1.614\mathrm{i}-2.555E^{1/2}$	$1.011\mathrm{i}-4.888E^{1/2}$	$0.699\mathrm{i}-8.407E^{1/2}$
2×10^{-3}	$1.607\mathrm{i}-2.001E^{1/2}$	$1.007\mathrm{i}-3.602E^{1/2}$	$0.698\mathrm{i}-5.783E^{1/2}$
1×10^{-3}	$1.603\mathrm{i}-1.734E^{1/2}$	$1.004\mathrm{i}-2.974E^{1/2}$	$0.696\mathrm{i}-4.499E^{1/2}$
5×10^{-4}	$1.599\mathrm{i}-1.549E^{1/2}$	$1.003\mathrm{i}-2.538E^{1/2}$	$0.696\mathrm{i}-3.612E^{1/2}$
2×10^{-4}	$1.596\mathrm{i}-1.388E^{1/2}$	$1.002\mathrm{i}-2.155E^{1/2}$	$0.695\mathrm{i}-2.836E^{1/2}$
1×10^{-4}	$1.594\mathrm{i}-1.308E^{1/2}$	$1.001\mathrm{i}-1.967E^{1/2}$	$0.695\mathrm{i}-2.452E^{1/2}$
5×10^{-5}	$1.593\mathrm{i}-1.253E^{1/2}$	$1.001\mathrm{i}-1.837E^{1/2}$	$0.695\mathrm{i}-2.183E^{1/2}$
2×10^{-5}	$1.592\mathrm{i}-1.206E^{1/2}$	$1.001\mathrm{i}-1.728E^{1/2}$	$0.695\mathrm{i}-1.943E^{1/2}$
1×10^{-5}	$1.592\mathrm{i}-1.181E^{1/2}$	$1.000\mathrm{i}-1.723E^{1/2}$	$0.695\mathrm{i}-1.815E^{1/2}$
Wedemeyer's estimate	$-1.201E^{1/2}$	$-1.590E^{1/2}$	$-1.591E^{1/2}$
Kudlick's estimate	$-1.119E^{1/2}$	$-1.512E^{1/2}$	$-1.532E^{1/2}$

TABLE 3. Frequencies $\sigma = \mathrm{i}\lambda + E^{1/2}s$ for $d = 1.9121$, $m = 1$ and $l = 2$

dimensional with an $E^{1/2}$ Ekman boundary layer present in each variable r and z, and the complicated corner region to resolve at their join. The low-Ekman-number results presented in tables 1–5 are produced by runs performed at truncations of $N = M = 35$ for $m \neq 0$ and $N = M = 40$ at $m = 0$, i.e. eigenvalues are found of double complex matrices of size 2450×2450 and double real matrices 3200×3200. These represent

E	$n=1$	$n=2$	$n=3$
5×10^{-3}	$0.985\mathrm{i}-3.840E^{1/2}$	$0.597\mathrm{i}-6.791E^{1/2}$	$0.410\mathrm{i}-11.109E^{1/2}$
2×10^{-3}	$0.978\mathrm{i}-3.084E^{1/2}$	$0.596\mathrm{i}-4.917E^{1/2}$	$0.425\mathrm{i}-7.665E^{1/2}$
1×10^{-3}	$0.973\mathrm{i}-2.717E^{1/2}$	$0.594\mathrm{i}-4.001E^{1/2}$	$0.425\mathrm{i}-5.907E^{1/2}$
5×10^{-4}	$0.970\mathrm{i}-2.465E^{1/2}$	$0.593\mathrm{i}-3.370E^{1/2}$	$0.424\mathrm{i}-4.687E^{1/2}$
2×10^{-4}	$0.967\mathrm{i}-2.246E^{1/2}$	$0.592\mathrm{i}-2.819E^{1/2}$	$0.424\mathrm{i}-3.634E^{1/2}$
1×10^{-4}	$0.966\mathrm{i}-2.139E^{1/2}$	$0.592\mathrm{i}-2.547E^{1/2}$	$0.424\mathrm{i}-3.105E^{1/2}$
5×10^{-5}	$0.965\mathrm{i}-2.062E^{1/2}$	$0.591\mathrm{i}-2.355E^{1/2}$	$0.424\mathrm{i}-2.740E^{1/2}$
2×10^{-5}	$0.964\mathrm{i}-1.993E^{1/2}$	$0.591\mathrm{i}-2.188E^{1/2}$	$0.424\mathrm{i}-2.418E^{1/2}$
1×10^{-5}	$0.963\mathrm{i}-1.971E^{1/2}$	$0.591\mathrm{i}-2.072E^{1/2}$	$0.424\mathrm{i}-2.275E^{1/2}$
Wedemeyer's estimate	$-2.167E^{1/2}$	$-2.088E^{1/2}$	$-2.001E^{1/2}$
Kudlick's estimate	$-1.881E^{1/2}$	$-1.901E^{1/2}$	$-1.866E^{1/2}$

TABLE 4. Frequencies $\sigma = \mathrm{i}\lambda + E^{1/2}s$ for $d = 1.35045$, $m = 2$ and $l = 1$

E	$n=1$	$n=2$	$n=3$
5×10^{-3}	$1.071\mathrm{i}-3.659E^{1/2}$	$0.648\mathrm{i}-6.301E^{1/2}$	$0.454\mathrm{i}-10.355E^{1/2}$
2×10^{-3}	$1.059\mathrm{i}-2.999E^{1/2}$	$0.640\mathrm{i}-4.648E^{1/2}$	$0.453\mathrm{i}-7.172E^{1/2}$
1×10^{-3}	$1.053\mathrm{i}-2.676E^{1/2}$	$0.636\mathrm{i}-3.841E^{1/2}$	$0.450\mathrm{i}-5.583E^{1/2}$
5×10^{-4}	$1.048\mathrm{i}-2.451E^{1/2}$	$0.634\mathrm{i}-3.281E^{1/2}$	$0.448\mathrm{i}-4.484E^{1/2}$
2×10^{-4}	$1.044\mathrm{i}-2.255E^{1/2}$	$0.632\mathrm{i}-2.791E^{1/2}$	$0.447\mathrm{i}-3.528E^{1/2}$
1×10^{-4}	$1.042\mathrm{i}-2.156E^{1/2}$	$0.631\mathrm{i}-2.547E^{1/2}$	$0.446\mathrm{i}-3.052E^{1/2}$
5×10^{-5}	$1.041\mathrm{i}-2.088E^{1/2}$	$0.631\mathrm{i}-2.375E^{1/2}$	$0.446\mathrm{i}-2.718E^{1/2}$
2×10^{-5}	$1.040\mathrm{i}-1.935E^{1/2}$	$0.630\mathrm{i}-2.222E^{1/2}$	$0.446\mathrm{i}-2.423E^{1/2}$
1×10^{-5}		$0.630\mathrm{i}-2.211E^{1/2}$	$0.446\mathrm{i}-2.269E^{1/2}$
Wedemeyer's estimate	$-1.923E^{1/2}$	$-1.964E^{1/2}$	$-1.919E^{1/2}$
Kudlick's estimate	$-1.923E^{1/2}$	$-1.964E^{1/2}$	$-1.919E^{1/2}$

TABLE 5. Frequencies $\sigma = \mathrm{i}\lambda + E^{1/2}s$ *for* $d = 1.35045$, $m = 0$ and $l = 1$. The asymptotic estimates are the same because $m = 0$

N	$E=10^{-4}$	$E=10^{-5}$
16	−1.5676	−1.5203
20	−1.5729	−1.3117
24	−1.5676	−1.6533
28	−1.5667	−1.4737
30	−1.5664	−1.4911
33	−1.5664	−1.4818
35	−1.5665	−1.4834

TABLE 6. The convergence of decay rates for $d = 1.9898$, $m = l = n = 1$ with truncation $N = M$

maximal truncations in terms of both storage – 300 MBytes – and CPU time – 3 days on a Sun SparcCenter 2000 machine running at 13 Mflops. Fortunately, the decay rates obtained at these truncations appear converged to three decimal places at $E = 10^{-4}$ and two decimal places at $E = 10^{-5}$, see table 6.

Not surprisingly, the pointwise convergence of the associated eigenfunctions is nowhere near so good, with spurious oscillations generally appearing in the interior near the axis as the Ekman number decreases much below 10^{-2}. In a way, this is to be anticipated as all the effort of the spectral expansions goes into accurately reproducing

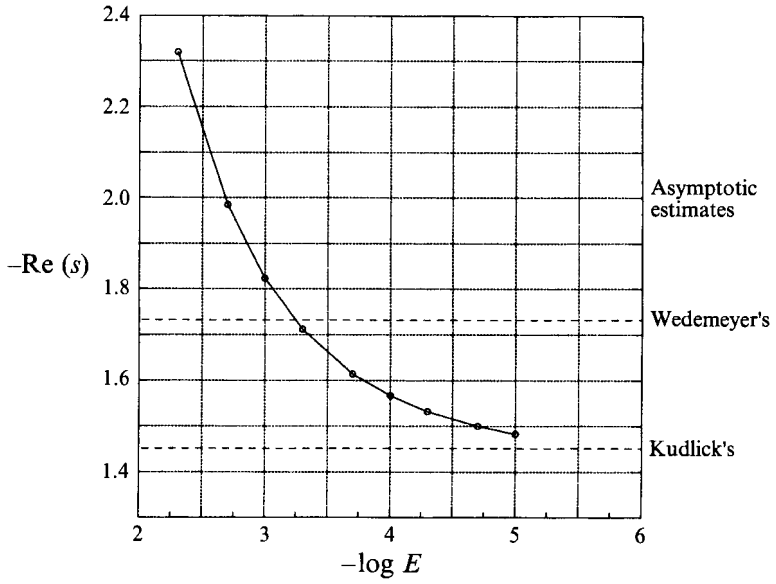

FIGURE 2. A plot of the numerical decay rate against Ekman number for the lowest ($l = n = 1$) subharmonic resonance $m = (-1, +1)$ at $d = 1.9898$ – see table 1.

the gradients at the boundary where the collocation points are dense. By design, this produces a 'good' decay rate estimate but, invariably, the solution away from the boundaries suffers as a consequence. Contour plots of the eigenfunctions attempt to reproduce the expected inertial wave structure with boundary layers but generally have not proved enlightening due to this lack of resolution: hence they are not shown. In particular, we have been unable to numerically identify the presence of viscous shear layers emanating from the corners. Recent numerical work in spherical shells (Hollerbach & Kerswell 1994) has illustrated how the well-known eruptions of Ekman boundary layers spawn internal shear layers. It seems likely that the corner regions of a cylinder behave in a similar fashion.

As is to be expected, all the viscous decay results displayed in tables 1–5 show a monotonic decline towards a limiting value which scales with $E^{1/2}$ as the Ekman number is reduced. In some cases, the numerical value at $E = 10^{-5}$ already undercuts Wedemeyer's asymptotic estimate: table 1, $n = 1$ is a particularly good example of this – see figure 2. These results clearly favour Kudlick's estimate. In other cases, the asymptotic regime has still to be reached, with the numerical value still well adrift from the asymptotic estimates at $E = 10^{-5}$. With hindsight, this is not surprising. Just considering the contribution to the decay rate from the interior suggests a corrective term of $O(E)$ with a coefficient containing the sum of the wavenumbers squared. As a result, an Ekman number of at most 10^{-4} is probably required for the corrective term to be just an order of magnitude smaller for a mode with wavenumbers of $O(\sqrt{10})$.

Our results support two conclusions. First, Kudlick's asymptotic decay rate expression appears the better *estimate* for the limiting decay rate value indicated by our numerical results suggesting that the corners *are* important. That it still remains an estimate is clear from the rather arbitrary smoothing of the corner regions employed in his derivation. Uncertainties in the corner region, particularly the possibility of internal shear layers, give no reason for expecting coincidence of Kudlick's estimate and the numerical decay rate asymptote. Secondly, although the correspondence can

be good for low-wavenumber modes, even Ekman numbers of 10^{-5} might not be small enough to ensure that Kudlick's asymptotic result is a good (within 10%) estimate of the actual viscous decay rate.

We would like to thank Dr T. J. Ratcliffe of the Newcastle University Computer Service for his patience and tolerance of the memory-intensive program runs performed during the course of this work on 'Aidan', the main university time-sharing computer.

REFERENCES

ALDRIDGE, K. D. & STERGIOPOULOS, S. 1991 A technique for direct measurement of time-dependent complex eigenfrequencies of waves in fluids. *Phys. Fluids* A **3**, 316–327.

BAINES, P. G. 1967 Forced oscillations of an enclosed rotating fluid. *J. Fluid Mech.* **30**, 533–546.

BJERKNES, V., BJERKNES, J., SOLBERG, H. & BERGERON, T. 1933 *Physikalische Hydrodynamik*, pp. 465–471. Springer.

FULTZ, D. 1959 A note on overstability, and the elastoid-inertia oscillations of Kelvin, Solberg and Bjerknes. *J. Met.* **16**, 199–208.

GANS, R. F. 1970 On the precession of a resonant cylinder. *J. Fluid Mech.* **41**, 865–872.

GREENSPAN, H. P. 1968 *The Theory of Rotating Fluids*. Cambridge University Press.

HOLLERBACH, R. 1994 Magnetohydrodynamic Ekman and Stewartson layers in a rotating spherical shell. *Proc. R. Soc. Lond.* A **444**, 333–346.

HOLLERBACH, R. & KERSWELL, R. R. 1994 Oscillatory, internal shear layers in rotating and precessing flows. *J. Fluid Mech.* (submitted).

JOHNSON, L. E. 1967 The precessing cylinder. In *Notes on the 1967 Summer Study Program in Geophysical Fluid Dynamics at the Woods Hole Oceanographic Inst. Ref.* 67-54, pp. 85–108.

KARPOV, B. G. 1965 Dynamics of a liquid-filled shell: resonance and the effects of viscosity. *BRL Rep.* 1302. US Army Ballistic Research Laboratory, Aberdeen Proving Ground, Maryland AD468654.

KELVIN, LORD 1880 Vibrations of a columnar vortex. *Phil. Mag.* **10**, 155–168.

KERSWELL, R. R. 1994*a* Tidal excitation of hydromagnetic waves and their damping in the Earth. *J. Fluid Mech.* **274**, 219–241.

KERSWELL, R. R. 1994*b* On the internal shear layers spawned by the critical regions in oscillatory Ekman boundary layers. *J. Fluid Mech.* (submitted).

KUDLICK, M. 1966 On the transient motions in a contained rotating fluid. PhD thesis, MIT.

MALKUS, W. V. R. 1989 An experimental study of the global instabilities due to the tidal (elliptical) distortion of a rotating elastic cylinder. *Geophys. Astrophys. Fluid Dyn.* **48**, 123–134.

MALKUS, W. V. R. & WALEFFE, F. A. 1991 Transition from order to disorder in elliptical flow: a direct path to shear flow turbulence. In *Advances in Turbulence 3* (ed. A. V. Johansson & P. H. Alfredsson), pp. 197–203. Springer.

MANASSEH, R. 1992 Breakdown regimes of inertia waves in a precessing cylinder. *J. Fluid Mech.* **243**, 261–296.

MANASSEH, R. 1994 Distortions of inertia waves in a rotating fluid cylinder forced near its fundamental mode resonance. *J. Fluid Mech.* **265**, 345–370.

MCEWAN, A. D. 1970 Inertial oscillations in a rotating fluid cylinder. *J. Fluid Mech.* **40**, 603–640.

STERGIOPOULOS, S. & ALDRIDGE, K. D. 1982 Inertial waves in a fluid partially filling a cylindrical cavity during spin-up from rest. *Geophys. Astrophys. Fluid Dyn.* **21**, 89–112.

STERGIOPOULOS, S. & ALDRIDGE, K. D. 1987 Ringdown of inertial waves during spin-up from rest of a fluid contained in a rotating cylindrical cavity. *Phys. Fluids* **30**, 302–311.

STEWARTSON, K. 1959 On the stability of a spinning top containing fluid. *J. Fluid Mech.* **5**, 577–592.

WEDEMEYER, E. H. 1966 Viscous corrections to Stewartson's stability criterion. *BRL Rep.* 1325. US Army Ballistic Research Laboratory, Aberdeen Proving Ground, Maryland AD489687.

WHITING, R. D. & GERBER, N. 1980 Dynamics of liquid-filled gyroscope: update of theory and experiment. *Rep. ARBRL-TR*-02221. US Army Ballistic Research Laboratory, Aberdeen Proving Ground, Maryland AD489687.

WOOD, W. W. 1965 Properties of inviscid, recirculating flows. *J. Fluid Mech.* **22**, 337–346.

WOOD, W. W. 1966 An oscillatory disturbance of rigidly rotating fluid. *Proc. R. Soc. Lond.* A **293**, 181–212.